Fault Diagnosis for Power Cables Based on Convolutional Neural Network With Chaotic System and Discrete Wavelet Transform

Meng-Hui Wang, *Member, IEEE*, Shiue-Der Lu, *Member, IEEE*, and Rui-Min Liao

***Abstract*—In this paper, the discrete wavelet transform (DWT) and a chaotic system were combined with a convolutional neural network (CNN) and applied to the diagnosis of insulation faults in XLPE (cross-linked polyacetylene) power cables. First, four different types of insulation faults in power cables were constructed, including the normal state of the cable, the short outer semiconducting layer, impurities in the insulation layer, and insulation layer damage, and a high-speed capture card (NI PXI-5105) was adopted to measure the partial discharge (PD) signal, which was then filtered through discrete wavelet transform. Then, based on the Lorenz chaotic system, a dynamic error scatter diagram was established as the feature of each fault state. Finally, the dynamic error scatter diagram was processed by CNN to recognize four different types of faults in the power cable. The test results show that the method proposed in this paper can quickly recognize the fault state of power cables and has excellent performance in terms of recognition accuracy, which reaches 97.5%. Therefore, the proposed method can effectively detect the fault signal changes of power cables and identify the fault state of power cables in real time.**

***Index Terms*—Discrete wavelet transform, chaotic system, convolutional neural networks, power cable, fault diagnosis, partial discharge.**

I. Introduction

ACCORDING to analysis of power cable faults, the faults resulting from the insulation damage of power cables due to poor human construction quality account for a considerable proportion of the total power cable faults [1]. Once the power cable insulation is faulted, it faces the high risk of power interruption at any time. Partial discharge (PD) is the main factor that causes insulation breakdown of high-voltage power equipment, and is an important indicator of equipment insulation deterioration. Therefore, the stability and safety of power systems will be greatly improved if the partial discharge state that exists in power cables can be detected at an early stage.

Manuscript received October 20, 2020; revised January 31, 2021; accepted March 3, 2021. Date of publication March 11, 2021; date of current version January 24, 2022. This work was supported by the Ministry of Science and Technology of Taiwan, under Contracts MOST 109-2221-E-167-009 and MOST 108-2221-E-167-018-MY2. Paper no. TPWRD-01547-2020. *(Corresponding author: Shiueder Lu.)*

The authors are with the Department of Electrical Engineering, National Chin-Yi University of Technology, Taichung 41170, Taiwan (e-mail: wangmh@ncut.edu.tw; sdl@ncut.edu.tw; seanliao0824@gmail.com).

Color versions of one or more figures in this article are available at https://doi.org/10.1109/TPWRD.2021.3065342.

Digital Object Identifier 10.1109/TPWRD.2021.3065342

In the traditional detection method of partial discharge, the features of the partial discharge signal are analyzed through pattern recognition [2], [3], which relies heavily on experienced experts, in order to effectively detect insulation faults. In recent years, with the rise of machine learning and artificial intelligence, different diagnostic methods for partial discharge have been proposed; for example, Hao *et al*. [4] used the support vector machine (SVM) in the data training and recognition of three artificial partial discharge models, which can effectively classify partial discharges. Mazzetti et al. [5] extracted the various features of partial discharge signals and an adaptive fuzzy neural network was used to diagnose the faults of power cables. Raymond et al. [6] Dimensionality reduction was carried out using principal Components analysis (PCA) to analyze the partial discharge data of five types of faults in power cables, as obtained by phase-resolved partial discharge (PRPD) [7], and the dimensionality reduction data was input into the classifier to identify the features. Meanwhile, the PCA feature extraction method was compared with traditional statistical feature extraction and fractal feature extraction methods, and these three features were input into a back propagation neural network (BPNN) and SVM to compare identification accuracy. The test results show that the PCA method is superior to the statistical and fractal feature extraction methods in identification in a high-noise environment, and SVM has higher recognition accuracy than BPNN. In addition, a breakthrough in image recognition technology recognizes different types of partial discharges with the image feature extraction method in the detection of power equipment. Firuzi et al. [8] converted the PRPD images of different partial discharge types into grayscale images, followed by feature extraction using the traditional methods of local binary pattern (LBP) and histogram of oriented gradient (HOG). Finally, the SVM classifier was used to identify partial discharge types.

This paper combined the discrete wavelet transform (DWT) [9]–[11], the Lorenz chaotic system, and a convolutional neural network (CNN) [12] to identify the insulation faults of four types of power cables. During identification, the partial discharge signal detected by HFCT was filtered by discrete wavelet and input into the Lorenz chaotic system to draw the dynamic error scatter diagram, and the image features were extracted and identified by CNN. Meanwhile, the proposed method was compared with the traditional HOG image feature extraction method with SVM

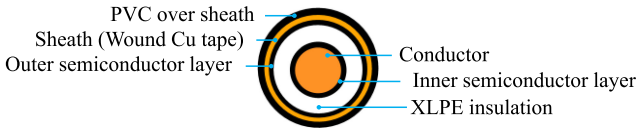

Fig. 1. Composition structure of power cables.

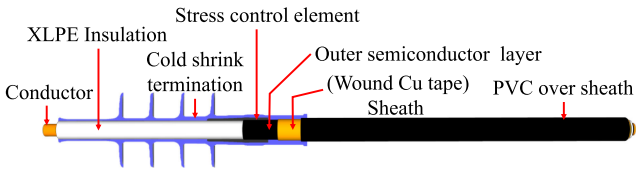

Fig. 2. Model of normal power cables.

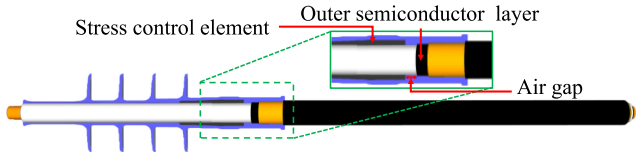

Fig. 3. Schematic of faults in the outer semi-conductive layer of power cables.

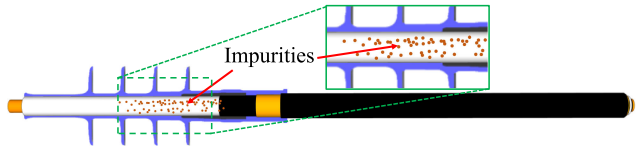

Fig. 4. Schematic for impurities in the insulation layer of power cables.

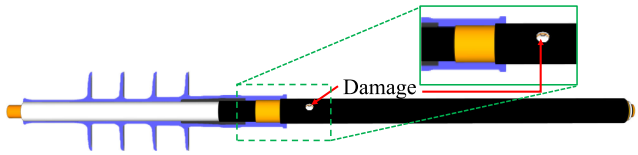

Fig. 5. Schematic for insulation damage of power cables.

[13], [14], BPNN [15], and K-Nearest Neighbor (KNN) [16], [17] classifiers for identification accuracy. The results show that the proposed method can effectively identify the partial discharge type of power cables and has the highest identification accuracy.

II. Partial Discharge Test of Power Cable

During the partial discharge detection process, the partial discharge signal measured by a sensor is inevitably interfered with by the surrounding environment or affected by the detection equipment, which increases detection difficulties. Therefore, in order to improve signal analysis and recognition, the signal analysis method is adopted to filter out the noise interference of the detected signal. The test process of partial discharge of power cables in this paper includes the construction of power cable faults, and the acquisition of partial discharge signals, as follows:

A. Construction of Power Cable Faults

In order to study the partial discharge in power cables, the single-core 25kV XLPE power cable with a cross-sectional area of 38 mm^2 is taken as the subject in this study. Fig. 1 shows the composition structure of the power cable, including the copper conductor, semi-conductor, insulator, shielding copper belt, and outer coating. The four common fault models for power cables are as follows:

1) Normal Power Cables (Type I): Before operating power cables, each layer of material must be peeled off respectively according to the construction regulations to avoid short circuits, as caused by the close distance between the copper conductor and ground. In addition, a terminal joint must be added to increase the surface distance to prevent high voltage creepage on the cable surface, as its wavy structure means that surface discharge accidents can be effectively avoided. Moreover, its stress cone can effectively distribute the electric field evenly. The normal power cable model established in this paper is shown in Fig. 2.

2) Short Outer Semi-Conducting Layer (Type II): Installation of terminal joints for power cables must be in accordance with the instructions of the manufacturer. If the construction code is not followed, the stress cone in the terminal joint cannot be located on the outer semi-conductive layer, resulting in the uneven distribution of the dielectric constant and electric field inside the terminal joint, thus, leading to partial discharge. Therefore, the fault model of power cables, as constructed in this paper, is shown in Fig. 3.

3) Impurities in the Insulation Layer (Type III): Some impurities may remain on the insulation layer due to the construction environment or natural dust during the installation of the terminal joint of power cables. In accordance with the construction regulations of power cables, special cleaning sheets must be used to wipe the insulation layer in a fixed direction, in order to prevent residual impurities on the insulation layer from affecting the distribution of the electric field. The fault model constructed in this paper simulates the impurities on the insulation layer, as shown in Fig. 4.

4) Insulation Layer Damage (Type IV): Power cables may suffer insulation damage due to external factors during installation, maintenance, removal, and operation. Severe damage to the insulation of power cables may be caused by digging with mechanical tools during construction or biting by animals. After the insulation layer is damaged, even if there is no immediate power interruption, water and gas will permeate into the insulation layer during long-term operation, which will eventually lead to insulation breakdown and a fault. This paper used a PCB bit with a diameter of 2mm to destroy half of the insulation layer, and the partial discharge was detected. The model is shown in Fig. 5.

B. Acquisition and Processing of Partial Discharge Signal

Fig. 6 is the test flow chart of the power cable designed in this paper. In order to generate a high voltage that reaches 22.8kV during the acquisition of a partial discharge signal, an

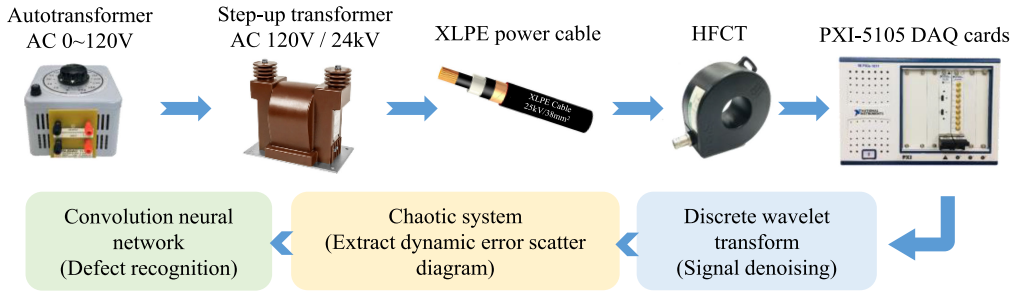

Fig. 6. Partial discharge test flowchart of power cables.

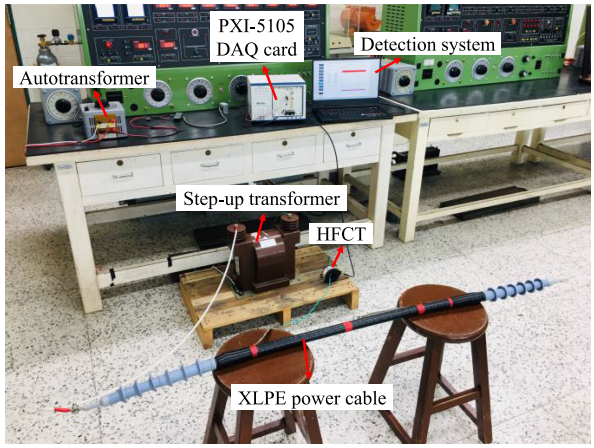

Fig. 7. Power cable test platform.

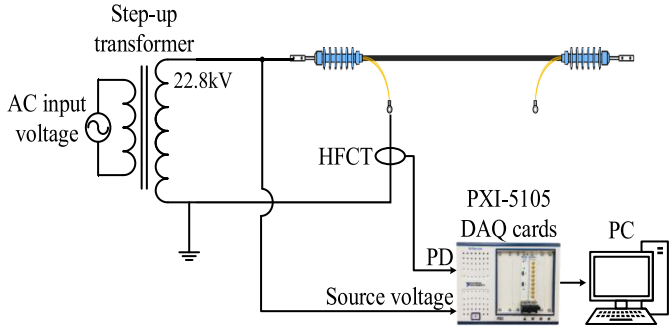

Fig. 8. Schematic diagram of partial discharge test setup.

auto transformer is used to adjust the voltage of the step-up transformer, which is then applied to the XLPE power cable conductor. In addition, the high frequency current transformer (HFCT) is connected to the power cable ground to sense the current pulse signal of the power cable ground. Then, a high-speed data acquisition card is adopted to receive the signal output by the high frequency current transformer for online analysis.

Fig. 7 shows the experimental environment in this study, where the bandwidth of HFCT is between 1 MHz and 60 MHz, and the sampling frequency of the NI PXI-5105 high-speed data acquisition card is 60 MHz, with 12bit resolution and 8 synchronous channels, which is enough to completely present the partial discharge signal detected by HFCT. This study used LabVIEW to design the human-machine interface to store and detect PD data. Additionally, the partial discharge test environment is represented as a schematic diagram, as shown in Fig. 8.

The acquired partial discharge signal is shown in Fig. 9. The cycle of the captured partial discharge signal equals three cycles of a 60 Hz power source, the sampling rate is 20MS/s, the measurement time is 50 ms, and 1 million pieces of data are acquired.

III. Methodology

A. Wavelet Transform of Signal

The purpose of signal processing is to obtain the features of the signal from different angles through different transform methods to assist in signal analysis and processing. The wavelet function is a new foundation for expressing signals, while the wavelet transform, which is also a time-frequency analysis technology that features a time-frequency elastic window, is a method for analyzing the signal from different resolutions.

Wavelet transform is divided into continuous wavelet transform (CWT) and discrete wavelet transform (DWT). As DWT is often used to suppress signal noises [18], it is applied in this paper to process the captured partial discharge signal.

The discrete wavelet can be expressed by (1).

$$\psi_{m,k}\ (t) = \frac{1}{\sqrt{2^m}}\ \psi\left(\frac{t-k}{2^m}\right) \tag{1}$$

Where m and k are the Scale parameter and Translation parameter, respectively. t is the time, $\psi_{m,k}(t)$ is the wavelet transform coefficient, and $\psi(t)$ is the base mother wavelet.

Input signals, which consist of low-frequency (LF) and high-frequency (HF) components, can be decomposed into frequency bands through DWT. Then, through down-sampling, the first level of wavelet transform can be obtained. The maximum number of decomposition layers in a wavelet transform is $\log_2 N$, where N is the length of the signal.

According to the features of the discrete wavelet crossover filter bank, the frequency band of the approximate coefficient (low frequency) cAi and the detail coefficient (high frequency) cDi can be expressed by (2) and (3), respectively, where i is the number of decomposition layers.

$$cA_i = \left[0, \frac{f_s}{2^{i+1}}\right] \tag{2}$$

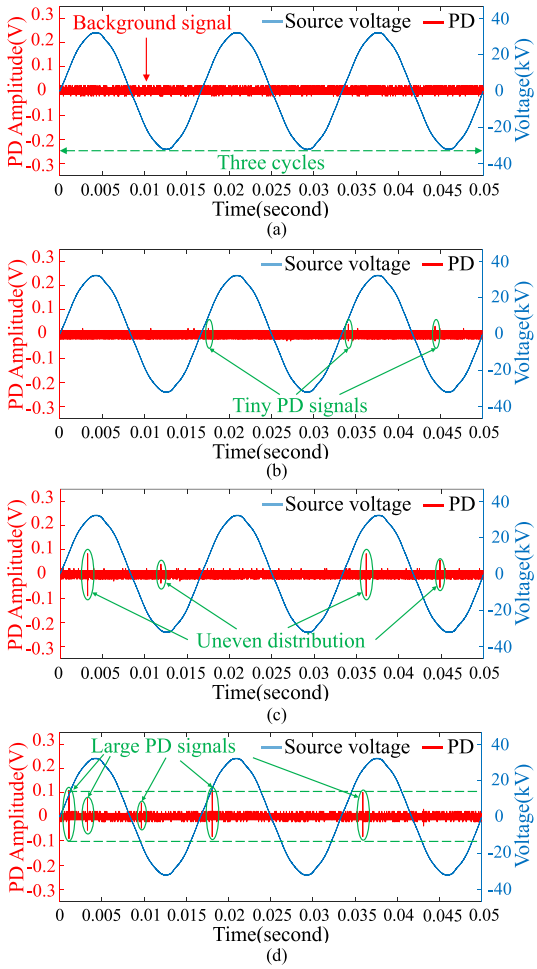

Fig. 9. Partial discharge signal of different insulation faults of power cable. (a) normal power cable, (b) short outer semiconductor layer, (c) impurities in the insulation layer, and (d) insulation layer damage.

$$cD_i = \left[\frac{f_s}{2^{i+1}}, \frac{f_s}{2^i}\right] \tag{3}$$

After the signal is decomposed, the original signal can be reconfigured by inverse discrete wavelet transform (IDWT) [19]. Since the signal has been down-sampled, it must be up-sampled during reconfiguration.

The following describes how the discrete wavelet is used to suppress noises:

1) Select the Number of Decomposition Layers: When discrete wavelet transform is adopted for signal filtering, generally, more decomposition layers can make it easier to separate the signal from the noise, which can yield a better filtering effect. However, if there are too many decomposition layers, the calculation time significantly increases, leading to unnecessary burdens.

In order to determine the number of decomposition layers of discrete wavelet transform, this study uses Fast Fourier Transform (FFT) [20] for spectral analysis of a partial discharge signal. The frequency range of the obtained partial discharge signal is 1 MHz to 10 MHz, as shown in Fig. 10.

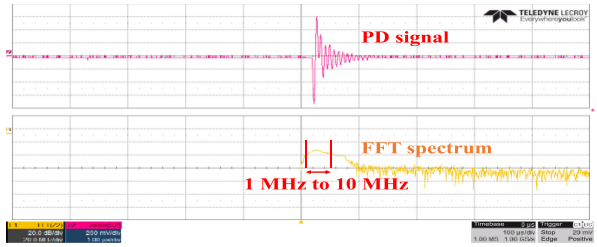

Fig. 10. Partial discharge signal and FFT spectrum.

TABLE I
FREQUENCY RANGE OF THE LAYERS DECOMPOSED BY DISCRETE WAVELET TRANSFORM

Number of decomposition layers	Approximate coefficient (low frequency) bandwidth (MHz)	Detail coefficient (high frequency) bandwidth (MHz)
1	cA1= [0, 5]	cD1= [5, 10]
2	cA2= [0, 2.5]	cD2= [2.5, 5]
3	cA3= [0, 1.25]	cD3= [1.25, 2.5]
4	cA4= [0, 0.625]	cD4= [0.625, 1.25]

This study employs a high-speed data acquisition card to measure the partial discharge signal of the power cable. The sampling frequency fs is set at 20 MHz, and the Nyquist-Shannon sampling theorem [21], [22] is applied herein. The highest measurable frequency of the partial discharge signal is 10 MHz in this study, and the bandwidth ranges of various hierarchies of discrete wavelet transform are decomposed by (2) and (3), as shown in Table I. Therefore, this study sets the number of decomposition layers of discrete wavelet transform as four, and the partial discharge signal of the high frequency part (0.625 MHz $\sim$ 10 MHz) is separated from various layers. The remaining low frequency signal (lower than 0.625 MHz) is background noise. Therefore, with the spectral analysis result of the partial discharge in Fig. 10, this study assigns the number of decomposition layers of discrete wavelet transform as four, so as to separate the partial discharge signal from the background noise effectively and to avoid excessive decomposition layers from increasing the operational load of the system.

2) Select the Mother Wavelet Function: Since the discrete wavelet transform filters out signals similar to the mother wavelet function, it is very important to select a mother wavelet similar to the partial discharge signal. The common mother wavelet functions include Haar wavelet, Coiflet wavelet, Daubechies (db) wavelet, and Symlets wavelet. Generally, in partial discharge studies, the oscillation-attenuated partial discharge pulse waveform is close to the Daubechies wavelet [23]. Therefore, in order to select the mother wavelet function that best fits the partial discharge signal, the Pearson correlation coefficient is used to calculate the correlation between the Daubechies wavelet function and the partial discharge pulse signal of the power cable. The Pearson correlation coefficient is expressed as:

$$\gamma = \frac{\sum (X - \bar{X})(Y - \bar{Y})}{\sqrt{\sum (X - \bar{X})^2 \sum (Y - \bar{Y})^2}} \tag{4}$$

where, X is the original partial discharge pulse signal, $\bar{X}$ is the average of the original partial discharge pulse signal, Y is the noise-eliminated discharge pulse signal, and $\bar{Y}$ is the average of the noise-eliminated discharge pulse signal.

3) Set the Threshold and Filter the Signal: After the mother wavelet is selected, the noise of the partial discharge signal can be filtered out. In this study, the Universal threshold is multiplied by the median of each decomposition layer after wavelet decomposition to automatically set the threshold, as shown in (5).

$$\lambda_j = \frac{\sigma_j}{0.6745} * \sqrt{2 \log n_j} \tag{5}$$

where, λ_j is the threshold of the j^{th} decomposition layer, σ_j is the median of the j^{th} decomposition layer, n_j is the signal length of the j^{th} decomposition layer.

After the threshold is set, the noise is filtered out through the threshold processing. The general threshold selection includes hard δ_λ^{Hard} and soft thresholds δ_λ^{Soft} [24].

Regarding the hard threshold, a larger wavelet coefficient is retained and the coefficient below the threshold is set to 0, as shown in (6).

$$\delta_\lambda^{Hard} = \begin{cases} x(t), \text{ if } |x(t)| > \lambda \\ 0, \text{ otherwise} \end{cases} \tag{6}$$

Regarding the soft threshold, the wavelet coefficient below the threshold is set to 0 and the coefficient greater than the threshold is reduced proportionally, as shown in (7).

$$\delta_\lambda^{Soft} = \begin{cases} \text{signal}(x(t))(|x(t)| - \lambda), \text{ if } |x(t)| > \lambda \\ 0, \text{ if } |x(t)| \le \lambda \end{cases} \tag{7}$$

In order to ensure that the complete partial discharge signal could be retained, this study applied the hard threshold to filter out the noise in the partial discharge signal. Finally, through IDWT, the signal processed by the hard threshold can be configured into a noise-eliminated partial discharge signal layer by layer. The original partial discharge signal ((a)∼(d) of Fig. 9), as measured by the power cable, was filtered by the discrete wavelet, as shown in Fig. 11.

After filtering, the partial discharge signal can be completely displayed, and the noise can be effectively suppressed.

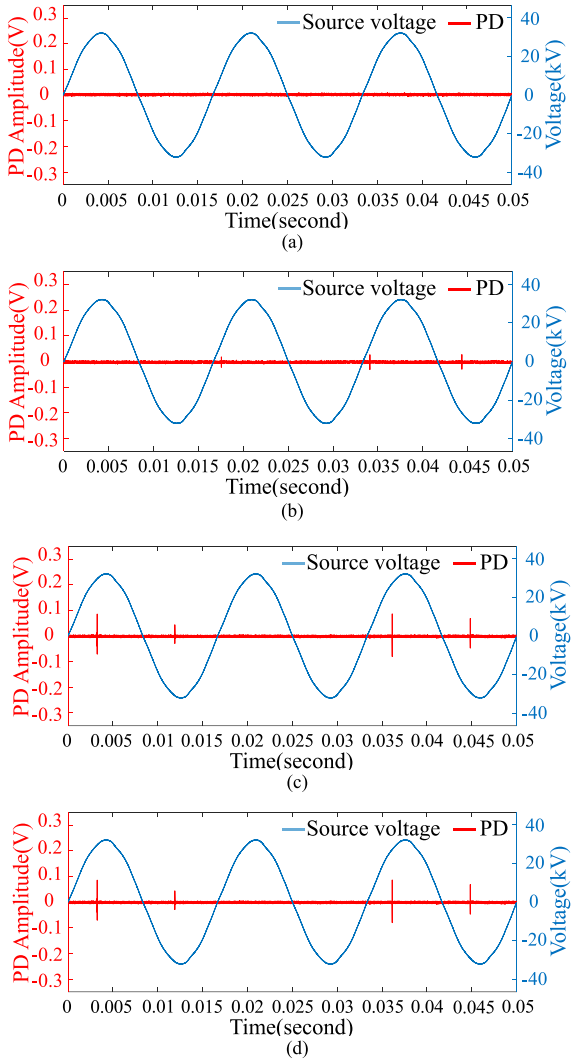

Fig. 11. Partial discharge signal after the different insulation faults of power cable are filtered out. (a) normal power cable, (b) short outer semiconductor layer, (c) impurities in the insulation layer, and (d) insulation layer damage.

B. Chaos Synchronization Detection Method

The Chaos Theory was proposed by an American meteorologist, Edward Norton Lorenz. The signal generated by the chaotic system produces an orderly movement trajectory without a fixed cycle due to the strange attractor, and the movement trajectory is greatly affected due to slight changes. The chaotic synchronization system mainly consists of a master system and a slave system. When the master system and the slave system receive different signals, the trajectories of the two systems produce different dynamic errors. If the slave system tracks the master system, it is called a chaotic synchronization action [25]. In this study, the dynamic error generated during the master-slave system tracking process is used to analyze the differences generated by different partial discharge faults.

The master and slave systems in this study are the partial discharge signals of normal and faulted power cables, and the generated dynamic errors can be drawn as a dynamic error scatter diagram. According to different power cable faults, the dynamic error scatter diagram shows different distributions and center positions (chaotic eye).

The master and slave systems of the chaotic system are expressed as (8) and (9), respectively. Where, x and y are state vectors, and $f(x)$ and $f(y)$ are nonlinear functions.

$$Master\ System = \begin{cases} \dot{x_1} = f_1(x_1, x_2, x_3, \cdots, x_n) \\ \dot{x_2} = f_2(x_1, x_2, x_3, \cdots, x_n) \\ \quad \vdots \\ \dot{x_n} = f_n(x_1, x_2, x_3, \cdots, x_n) \end{cases} \tag{8}$$

$$Slave\ System\ = \begin{cases} \dot{y_1} = f_1\left(y_1, y_2, y_3, \cdots, y_n\right) \\ \dot{y_2} = f_2\left(y_1, y_2, y_3, \cdots, y_n\right) \\ \quad \vdots \\ \dot{y_n} = f_n\left(y_1, y_2, y_3, \cdots, y_n\right) \end{cases} \tag{9}$$

By subtracting (8) from (9), we can obtain the master-slave dynamic error, which is expressed as (10), and the obtained dynamic error equation is shown in (11).

$$\begin{cases} e_1 = x_1 - y_1 \\ e_2 = x_2 - y_2 \\ \quad \vdots \\ e_n = x_n - y_n \end{cases} \tag{10}$$

$$\begin{cases} \dot{e}_1 = f_1\ \left(x_1, x_2, x_3, \cdots, x_n\right) - f_1\left(y_1, y_2, y_3, \cdots, y_n\right) \\ \dot{e}_2 = f_2\ \left(x_1, x_2, x_3, \cdots, x_n\right) - f_2\left(y_1, y_2, y_3, \cdots, y_n\right) \\ \quad \vdots \\ \dot{e}_n = f_n\ \left(x_1, x_2, x_3, \cdots, x_n\right) - f_n\left(y_1, y_2, y_3, \cdots, y_n\right) \end{cases} \tag{11}$$

The Lorenz Chaotic system is used to extract the features of a partial discharge signal from a power cable. The master and slave systems of the Lorenz Chaotic system are expressed as (12) and (13), respectively.

$$Lorenz\ Master\ System: \begin{cases} \dot{x}_1 = \alpha\left(x_2 - x_1\right) \\ \dot{x}_2 = \beta x_1 - x_1 x_3 - x_2 \\ \dot{x}_3 = x_1\ x_2 - \gamma x_3 \end{cases} \tag{12}$$

$$Lorenz\ Slave\ System: \begin{cases} \dot{y}_1 = \alpha\left(y_2 - y_1\right) \\ \dot{y}_2 = \beta y_1 - y_1 y_3 - y_2 \\ \dot{y}_3 = y_1\ y_2 - \gamma y_3 \end{cases} \tag{13}$$

This study feeds the partial discharge signals of a normal power cable and faulty power cable into the master system ((8)) and slave system ((9)), respectively. If *r* is the data sequence of the partial discharge signal of the normal power cable, and *s* is the data sequence of the partial discharge signal of the faulty power cable, then the parameters of (12) can be defined as $x_1 = r[u]$, $x_2 = r[u+1]$, and $x_3 = r[u+2]$, and the parameters of (13) are $y_1 = s[u]$, $y_2 = s[u+1]$, and $y_3 = s[u+2]$, where $u = 12, \ldots, v\text{-}2$, and v is the total amount of data of the partial discharge signal. Then the dynamic error calculated from (12) and (13) is expressed as (14) in the form of a matrix.

$$\begin{bmatrix} \dot{e}_1 \\ \dot{e}_2 \\ \dot{e}_3 \end{bmatrix} = \begin{bmatrix} -\alpha & \alpha & 0 \\ \beta & -1 & 0 \\ 0 & 0 & -\gamma \end{bmatrix} \begin{bmatrix} e_1 \\ e_2 \\ e_3 \end{bmatrix} + \begin{bmatrix} 0 \\ -e_1 e_3 \\ e_1 e_2 \end{bmatrix} \tag{14}$$

In the Lorenz dynamic error, α, β, and γ are system parameters. According to the experience of Edward Lorenz, the parameters of this system are set as $\alpha = 10$, $\beta = 28$, and $\gamma = 8/3$, to ensure the existence of the property of singular attractors in the chaotic system [26]. The dynamic error scatter diagram is drawn using vector e_1 as the X-coordinate and vector e_2 as the Y-coordinate according to the obtained dynamic error values e_1 and e_2. Fig. 12 illustrates the dynamic error scatter diagram, where the blue dot is the dynamic error, and the red dot represents the centroid position of the scatter diagram (chaotic eyes).

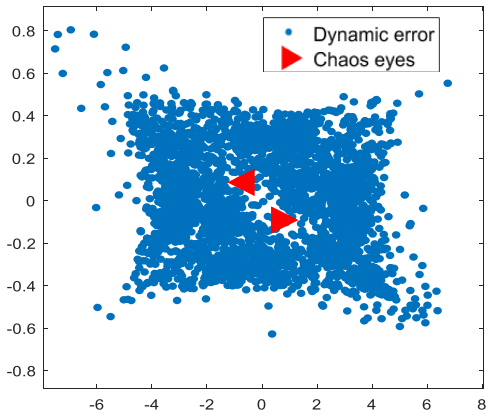

Fig. 12. Typical dynamic error scatter diagram.

C. Convolutional Neural Networks Work (CNN)

In recent years, CNN has been widely used in signal processing and image classification, such as face recognition [27], imaging medicine [28], fault diagnosis [29], etc., and it has yielded good application results. The CNN model design differs according to the features of the tested images. The main CNN architecture is basically composed of several convolutional layers, a pooling layer, a fully connected layer, and an activation layer.

This study designed a chaotic error scatter diagram that uses the convolutional neural network to identify the fault state of a power cable, and all images are 64 × 64pixel RGB images. The convolutional neural network model architecture is shown in Fig. 13 . The operation of each layer is described, as follows:

1) Convolutional Layer: The convolutional layer mainly extracts the features from the network, performs convolutional operations through masks of different sizes, and extracts or enhances the features of images by the concept of spatial filtering.

2) Pooling Layer: After the image features are obtained from the Convolutional layer, in order to effectively reduce the size of the feature parameters of the images and maintain the invariance of the features, a Pooling layer is added after the features are extracted, which can reduce the complexity of the overall network operation, and focus the pooled information on the consistency of the features. The common pooling methods include Max pooling and Average pooling.

3) Activation Layer: The main function of the activation layer is to enhance the non-linear characteristics of the network. The current common activation functions include Sigmoid, TanHyperbolic (tanh), and Rectified Linear Unit (ReLU) functions. The ReLU function can greatly improve the performance of CNN, and its performance in training speed is also better than that of other functions [30]. The ReLU function is expressed as (15).

$$f\ (k) = \max\left(0, k\right) \tag{15}$$

Where, *k* is the output of the previous neuron.

4) Fully Connected Layer: The architecture of the fully connected layer is mainly composed of flat layer, hidden layer, and output layer. The fully connected layer serves to obtain the results of the convolutional and pooling operation process, and

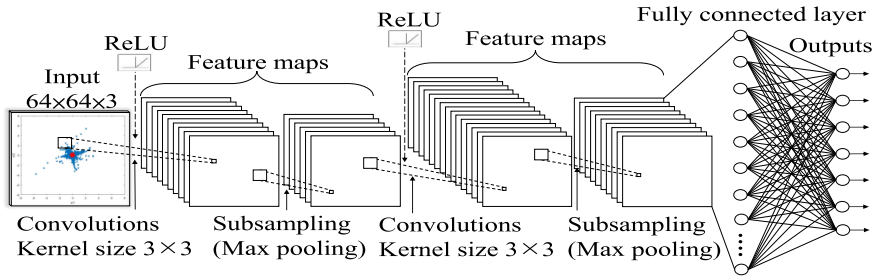

Fig. 13. The CNN architecture diagram designed in this paper.

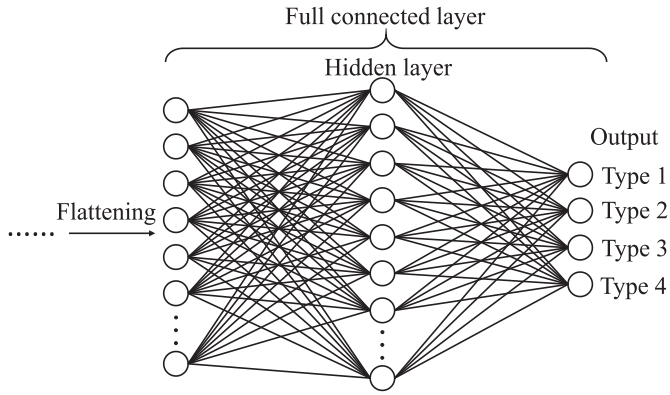

Fig. 14. Model architecture for fully connected layer.

TABLE II
RECOGNITION RESULTS OF INSULATION FAULTS OF POWER CABLES

Fault type	Test pattern	Accurate pattern	Recognizing rate (%)
Normal	90	89	97.5%
Short outer semiconductor layer	90	88	
Impurities in the insulation layer	90	85	
Insulation layer damage.	90	89	

then, predicts and classifies the images. Its structure is shown in Fig. 14.

IV. EXPERIMENTAL RESULTS

A. Dynamic Error Scatter Diagram

In this study, the partial discharge signals, as acquired by the power cable fault models, were filtered by DWT, and the data was input into the Lorenz Chaotic system for dynamic error calculation, and dynamic error e_1e_2 is used to generate dynamic error scatter diagram. The chaotic dynamic error scatter diagram for the four types of power cable faults is shown in Fig. 15.

The dynamic error scatter diagrams, as drawn under different fault states of power cables, show that the dynamic error scatter diagrams of different types of faults and their center have different distribution positions and densities. The distribution of normal and faultless power cables is concentrated, and when a cable insulation fault is more serious, the dynamic error scatter diagram will be more dispersed. Therefore, this feature was further applied in CNN training and recognition.

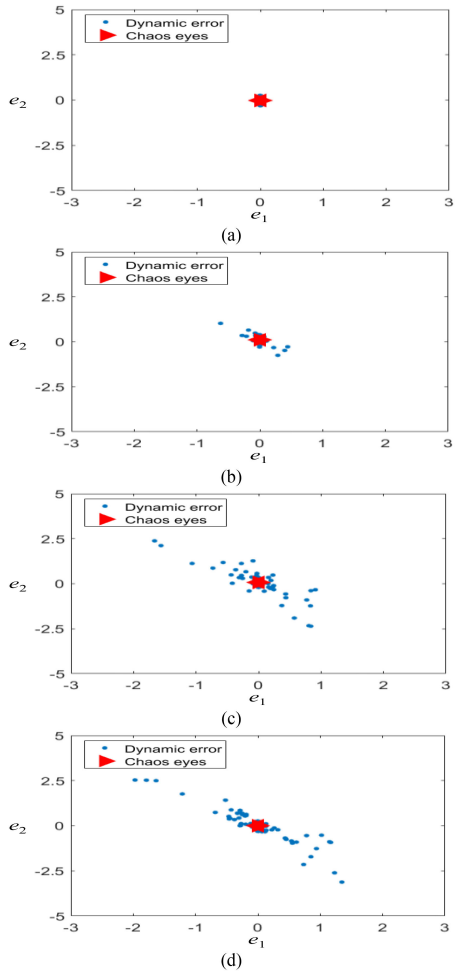

Fig. 15. Dynamic error scatter diagram for different types of power cable faults. (a) normal power cable, (b) short outer semiconductor layer, (c) impurities in the insulation layer, and (d) insulation layer damage.

B. CNN Fault Recognition

The CNN architecture used in this study has two convolutional layers, two pooling layers and one fully-connected layer, a 3×3 mask (convolution kernel), and a ReLu activation function that were used to identify the type of faults of power cables. The

TABLE III
COMPARISON OF RECOGNITION PERFORMANCE BETWEEN CNN AND TRADITIONAL DETECTION METHODS

Detection method	DWT filtering execution time (second)	Dynamic error execution time (second)	Training time (second)	Test time (second)	Recognition accuracy (%)		Ranking
					0% noise	10% noise	
CNN	162 (400 samples)	1586 (400 samples)	25	0.28	97.5	94.4	1
HOG+SVM			13	1.44	91.9	90.6	2
HOG+BPNN			90	1.63	88.6	83.9	3
HOG+KNN			11	1.46	85.6	85.3	4

test environment is MATLAB 2020a with Intel Core (TM) i7-9700 processor, NVIDIA GeForce RTX 2080 SUPER graphics card, along with Windows professional 64-bit operating system. The convolutional neural network model designed in this study uses the chaotic dynamic error scatter diagrams of power cables as the recognition sample. The CNN model for identifying the types of insulation faults of power cables was trained by 400 dynamic error scatter diagrams, and with 100 samples for each type of fault. In addition, in order to verify the validity of the CNN model to identify different types of power cable faults, 360 dynamic error scatter diagrams were used for testing, with 90 samples for each type of fault. According to the results in Table II, the proposed method can effectively classify different types of insulation faults of power cables, and has recognition accuracy of 97.5%.

The recognition performance of CNN and traditional image recognition detection methods for insulation fault types of power cables are compared in this study, and the results are shown in Table III. Discrete wavelet filtering and dynamic error operations are performed before CNN and the traditional detection method are used for model training. In terms of training time, while traditional HOG+SVM and HOG+KNN can complete the classifier training in a faster time, CNN can complete the training in only 25 seconds, and HOG+BPNN requires 90 seconds to complete the training, which is the most time-consuming among the four detection methods. Regarding recognition accuracy, CNN has 97.5% recognition accuracy, which is the highest among the four detection methods, followed by 91.9% for HOG+SVM, 88.6% for HOG+BPNN, and 85.6% for HOG+KNN. In addition, to validate the effectiveness and fault tolerance of the proposed method, 10% noise is added to the original unfiltered partial discharge signal, and the recognition accuracies of four detection methods are compared with the result shown in Table III. After the original signal is mixed with 10% noise, the recognition accuracy of CNN is 94.4%, which is the best performance among the four detection methods, meaning that the proposed method has excellent robustness.

C. Human-Machine Interface for Fault Diagnosis

The method proposed in this study is integrated into LabVIEW software to develop a fault diagnosis system, the interface of which is shown in Fig. 16.

In this system, the partial discharge data of power cables, as acquired by the high-speed data acquisition card, is stored in a personal computer, the file is read through the human-machine interface, and then, the chaotic system is used to draw the dynamic error scatter diagrams, as shown in part (a). Then, the trained CNN is used to recognize the faults, and the diagnosis result is displayed on the human-machine interface, as shown in part (b). The human-machine interface developed in this study can convert a signal into a Lorenz dynamic error scatter diagram immediately after measuring the partial discharge signal of a power cable, and the proposed method can be used for on-line intelligent diagnosis of insulation fault types of power cables, in order to effectively and quickly lock power cables with fault symptoms and carry out maintenance as soon as possible.

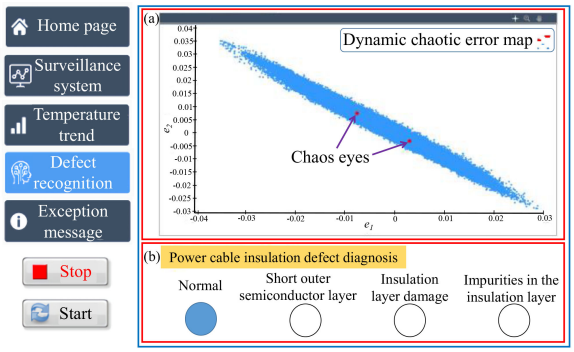

Fig. 16. Human-machine interface for fault diagnosis.

V. CONCLUSION

This paper proposed a fault recognition method for power cables, as based on wavelet transform, the chaotic system, and CNN. Specifically, four common types of power cable faults were constructed, and the Lorenz Chaotic system was used to draw the chaotic dynamic error scatter diagrams from the acquired data, which were taken as the fault diagnosis samples, and then, the trained CNN model was used to recognize the types of faults. Compared with the traditional HOG+SVM, HOG+BPNN, and HOG+KNN detection methods, the accuracy of the method proposed in this paper is 97.5%, which proves the effectiveness of the presented method.

The characteristics of the method proposed in this paper are, as follows:

- The chaotic dynamic error scatter diagrams, as generated by different types of faults, have unique distribution positions and densities, which is more conducive to the recognition of convolutional neural networks.

- The combined chaotic dynamic error scatter diagram and CNN can fully demonstrate the effectiveness of the method proposed in this paper, which has good recognition accuracy.
- Through the fault diagnosis human-machine interface established in this paper, the fault type identification of a power cable can be effectively and quickly carried out online, which makes the maintenance of power equipment more efficient.

REFERENCES

[1] C. Zhou, H. Yi, and X. Dong, "Review of recent research towards power cable life cycle management," *High Voltage*, vol. 2, no. 3, pp. 179–187, Sep. 2017.

[2] F. C. Gu, H. T. Yau, and H. C. Chen, "Application of chaos synchronization technique and pattern clustering for diagnosis analysis of partial discharge in power cables," *IEEE Access*, vol. 7, pp. 76185–76193, 2019.

[3] C. K. Chang, C. S. Lai, and R. N. Wu, "Decision tree rules for insulation condition assessment of pre-molded power cable joints with artificial defects," *IEEE Trans. Dielectrics Elect. Insul.*, vol. 26, no. 5, pp. 1636–1644, Oct. 2019.

[4] L. Hao and P. L. Lewin, "Partial discharge source discrimination using a support vector machine," *IEEE Trans. Dielectrics Elect. Insul.*, vol. 17, no. 1, pp. 189–197, Feb. 2010.

[5] C. Mazzetti, F. M. F. Mascioli, F. Baldini, M. Panella, R. Risica, and R. Bartnikas, "Partial discharge pattern recognition by neuro-fuzzy networks in heat-shrinkable joints and terminations of XLPE insulated distribution cables," *IEEE Trans. Power Del.*, vol. 21, no. 3, pp. 1035–1044, Jul. 2006.

[6] W. J. K. Raymond, H. A. Illias, and A. H. A. Bakar, "High noise tolerance feature extraction for partial discharge classification in XLPE cable joints," *IEEE Trans. Dielectrics Elect. Insul.*, vol. 24, no. 1, pp. 66–74, Feb. 2017.

[7] H. Janani and B. Kordi, "Towards automated statistical partial discharge source classification using pattern recognition techniques," *High Voltage*, vol. 3, no. 3, pp. 162–169, Sep. 2018.

[8] K. Firuzi, M. Vakilian, B. T. Phung, and T. R. Blackburn, "Partial discharges pattern recognition of transformer defect model by LPB & HOG features," *IEEE Trans. Power Del.*, vol. 34, no. 2, pp. 542–550, Apr. 2019.

[9] C. Lin, W. Gao, and M. F. Guo, "Discrete wavelet transform-based triggering method for single-phase earth fault in power distribution systems," *IEEE Trans. Power Del.*, vol. 34, no. 5, pp. 2058–2068, Oct. 2019.

[10] I. M. Karmacharya and R. Gokaraju, "Fault location in ungrounded photovoltaic system using wavelets and ANN," *IEEE Trans. Power Del.*, vol. 33, no. 2, pp. 549–559, Apr. 2018.

[11] T. M. Lai, L. A. Snider, E. Lo, and D. Sutanto, "High-impedance fault detection using discrete wavelet transform and frequency range and RMS conversion," *IEEE Trans. Power Del.*, vol. 20, no. 1, pp. 397–407, Jan. 2005.

[12] S. Wang and P. Dehghanian, "Power grid online surveillance through PMU-Embedded convolutional neural networks," *IEEE Trans. Ind. Appl.*, vol. 56, no. 2, pp. 1146–1155, Mar.-Apr. 2020.

[13] Y. Benmahamed, M. Teguar, and A. Boubakeur, "Application of SVM and KNN to duval pentagon 1 for transformer oil diagnosis," *IEEE Trans. Dielectrics Elect. Insul.*, vol. 24, no. 6, pp. 3443–3451, Dec. 2017.

[14] F. N. Rudsari, A. A. Razi-Kazemi, and M. A. Shoorehdeli, "Fault analysis of high-voltage circuit breakers based on coil current and contact travel waveforms through modified SVM classifier," *IEEE Trans. Power Del.*, vol. 34, no. 4, pp. 1608–1618, Aug. 2019.

[15] Y. Xie, J. Ruan, Y. Shi, S. Jin, Y. Tian, and L. Zhu, "Inversion detection method for resistivity of oil-immersed paper in transformer," *IEEE Trans. Power Del.*, vol. 34, no. 4, pp. 1757–1765, Aug. 2019.

[16] V. Basharan *et al.*, "Recognition of multiple partial discharge patterns by multi-class support vector machine using fractal image processing technique," *IET Sci., Meas. Technol.*, vol. 12, no. 8, pp. 1031–1038, Nov. 2018.

[17] M. Farshad and J. Sadeh, "Accurate single-phase fault-location method for transmission lines based on K-Nearest neighbor algorithm using one-end voltage," *IEEE Trans. Power Del.*, vol. 27, no. 4, pp. 2360–2367, Oct. 2012.

[18] I. Papadhopulli and B. Cico, "Implementation in FPGA of 3D discrete wavelet transform for imaging noise removal," *ICT Innov. 2012: Adv. Int. Syst. Comput.*, vol. 207, pp. 363–372, doi: 10.1007/978-3-642-37169-1_36

[19] B. F. Wu and Y. Q. Hu, "An efficient VLSI implementation of the discrete wavelet transform using embedded instruction codes for symmetric filters," *IEEE Trans. Circuits Syst. Video Technol.*, vol. 13, no. 9, pp. 936–943, Sep. 2019.

[20] S. Rapuano and F. J. Harris, "An introduction to FFT and time domain windows," *IEEE Instrum. Meas. Mag.*, vol. 10, no. 6, pp. 32–44, Dec. 2007.

[21] H. Nyquist, "Certain topics in telegraph transmission theory," *Trans. Amer. Inst. Elect. Engineers*, vol. 4, no. 2, pp. 617–644, Apr. 1928.

[22] C. E. Shannon and W. Weaver, *The Mathematical Theory of Communication*. Illinois, IL, USA: Univ. Illinois Press, 1998. [Online]. Available: https://www.press.uillinois.edu/books/catalog/67qhn3ym9780252725463.html

[23] X. ma, C. Zhou, and I. J. Kemp, "Interpretation of wavelet analysis and its application in partial discharge detection," *IEEE Trans. Dielectrics Elect. Insul.*, vol. 9, no. 3, pp. 446–457, Jun. 2002.

[24] R. Hussein, K. B. Shaban, and A. H. El-Hag, "Energy conservation-based thresholding for effective wavelet denoising of partial discharge signals," *IET Sci., Meas. Technol.*, vol. 10, no. 7, pp. 813–822, Oct. 2016.

[25] L. M. Pecora and T. L. Carroll, "Synchronization in chaotic systems," *Phys. Rev. Lett.*, vol. 64, no. 8, pp. 821–824, Feb. 1990.

[26] H. T. Yau and M. H. Wang, "Chaotic eye-based fault forecasting method for wind power systems," *IET Renewable Power Gener.*, vol. 9, no. 6, pp. 593–599, Oct. 2015.

[27] R. Ranjan *et al.*, "A fast and accurate system for face detection, identification, and verification," *IEEE Trans. Biometrics, Behav., Identity Sci.*, vol. 1, no. 2, pp. 82–96, Apr. 2019.

[28] S. Pereira, A. Pinto, V. Alves, and C. A. Silva, "Brain tumor segmentation using convolutional neural networks in MRI images," *IEEE Trans. Med. Imag.*, vol. 35, no. 5, pp. 1240–1251, May 2016.

[29] R. Liu, G. Meng, B. Yang, C. Sun, and X. Chen, "Dislocated time series convolutional neural architecture: An intelligent fault diagnosis approach for electric machine," *IEEE Trans. Ind. Informat.*, vol. 13, no. 3, pp. 1310–1320, Jun. 2017.

[30] Y. Wang, Y. Li, and X. Rong, "The influence of the activation function in a convolution neural network model of facial expression recognition," *Appl. Sci.*, vol. 10, no. 5, pp. 1–20. Mar. 2020.

Meng-Hui Wang (Member, IEEE) received the M.S. and Ph.D. degrees in electrical engineering from the National Taiwan University of Science and Technology, Taipei, Taiwan, in 1990 and 1994, respectively. In August 1994, he joined the National Chin-Yi University of Technology, Taichung, Taiwan and is currently affiliated with the Department of Electrical Engineering as a Lifetime Distinguished Professor. His main research interests include renewable energy systems, power systems, extension theory, and AI applications.

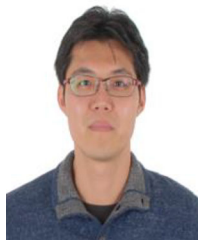

Shiue-Der Lu (Member, IEEE) received the M.S. degree from Chung Yuan Christian University and the Ph.D. degree from the National Taiwan University of Science and Technology, Taipei, Taiwan, in 2006 and 2013, respectively, both in electrical engineering. Since 2018, he has been with the Department of Electrical Engineering, National Chin-Yi University of Technology, Taichung, Taiwan, where he is currently an Associate Professor. His research interests include renewable energy, power systems, fault diagnosis, and optimization algorithm.

Rui-Min Liao received the M.S. degree from the Department of Electrical Engineering, National Chin-Yi University of Technology, Taichung, Taiwan, in 2020. His main research interests include artificial engineering and fault diagnosis.